Organizational principles of human and rodent association cortex

Mohan, H.

2017

document version
Publisher's PDF, also known as Version of record

Chapter 3
Functional architecture of posterior parietal cortex during tactile sensorimotor behavior

(in preparation)

Functional architecture of rat posterior parietal cortex during tactile sensorimotor behavior

Hemanth Mohan, Roel de Haan, Robin Broersen, Anton W. Pieneman, Keerthi Kumar Doreswamy, Huibert D. Mansvelder, Christiaan P.J. de Kock#

Department of Integrative Neurophysiology, Center for Neurogenomics and Cognitive Research, Neuroscience Campus Amsterdam, VU University Amsterdam, the Netherlands

Abstract

The posterior parietal cortex (PPC) in rodents is reciprocally connected to primary somatosensory cortex (S1) and vibrissal motor area (M2). PPC could thus bridge incoming sensory information to motor output but the cellular activity map across PPC layers during sensorimotor whisker behavior remains largely unknown. To uncover the functional architecture in PPC during active tactile processing, we performed single unit and ensemble recordings across cytoarchitectonic layers of PPC in anaesthetized and awake, behaving rats. In urethane-anaesthetized rats, mechanical (passive) whisker stimulation for receptive field measurements reveal whisker-related somatotopy, resembling S1 architecture but at lower spatial resolution. Juxtasomal single unit and silicon probe ensemble recordings in awake, behaving rats during whisking reveal efferent copy coding in PPC, reflected as increased spiking activity in PPC during self-induced exploratory whisking. Efferent copy encoding is layer-specific since spiking activity in superficial and deep layers is increased during free whisking, but not in middle layers. Furthermore, spiking activity in superficial and deep layers is tuned to whisker protraction in contrast to middle layers, where spiking is tuned to whisker retraction. Active object touch further induces spiking activity in individual units, indicating the integration of both efferent copy and ex-afference signals, and again, this integration is restricted to superficial and deep PPC layers. The cellular activity map of PPC during active tactile behavior therefore indicates layer-specific encoding of self-generated whisker movements and ex-afference information. We put forward the hypothesis that superficial and deep PPC layers serve as an integrative hub bridging sensory encoding in the PPC-S1 loop and motor output in the PPC-M2 projection.

Introduction

The dynamic interaction between external sensory (ex-afference) and internally generated motor information (efference copy) is crucial for sensorimotor behavior (Cullen 2004). The underlying circuitry involves sensory, motor and association cortices (Fries 2009; Chen et al. 2013; Chen et al. 2016). Of these cortical circuitries, the function and

cellular architecture of association cortices remains least understood. The rodent whisker system is an ideal system to reveal the neuronal mechanisms that govern sensorimotor behavior including self-induced whisker motion and processing of incoming tactile sensory information (de Kock et al. 2007; Petersen 2007; Diamond et al. 2008; Matyas et al. 2010; Hill et al. 2011; Friedman et al. 2012; Feldmeyer et al. 2013; Petersen 2014; Moore, Mercer Lindsay, et al. 2015; Hooks 2016). The primary somatosensory cortex (S1) has been the primary target for studying cortical representation of sensory information from the external world (ex-afference) whereas vibrissal motor cortex is studied in the context of rhythmic whisker movements (Brecht, Krauss, et al. 2004; Brecht, Schneider, et al. 2004; Diamond et al. 2008; Petersen 2014). Additionally, secondary sensory cortex and association cortices are thought to transform sensory information into downstream motor commands to generate appropriate context-specific behavior (Mountcastle et al. 1975; Gail and Andersen 2006; Cui and Andersen 2007; Andersen and Cui 2009).

Anatomical studies have revealed strong reciprocal axonal connectivity between S1 – PPC and feedforward projections from PPC to AGm/M1/vibrissal M2 (Colechio and Alloway 2009; Lee et al. 2011; Oberlaender et al. 2011; Wang et al. 2012; Smith and Alloway 2013). Thus, the rodent whisker system is ideal to study the involvement of PPC in sensorimotor (tactile) behavior. Here, we determined coding mechanisms of individual neurons across layers in rat PPC during tactile sensory processing (ex-afferent information) versus active motor behavior (efferent copy) (Cullen 2004). First, we used in vivo juxtasomal recordings in anaesthetized rats (Narayanan et al. 2014), to show functional somatotopy in PPC resembling somatotopy in the trigemino-thalamocortical pathway. Using juxtasomal single cell and silicon probe multiunit recordings in awake, head-fixed rats we show that self-induced whisker motion (efference copy) modulates layer specific spiking activity. We also show that activity in a subset of whisking-modulated neurons increase spiking upon active whisker touch. Finally, we show that spiking in middle PPC layers is tuned to whisker retraction in contrast to superficial and deep layers where spiking is tuned to whisker protraction. Individual PPC neurons are able to encode both whisker motion and whisker touch, which allows the PPC microcircuit to bridge incoming sensory information to appropriate motor output during tactile and/or multi-sensory processing (Olcese et al. 2013)\

Results

Spontaneous and evoked activity across PPC layers

We performed juxtasomal recordings of individual neurons across PPC layers of urethane anaesthetized rats (Pinault 1996; Narayanan et al. 2014) to characterize the organizational principles of PPC at cellular resolution. The location of PPC was de-

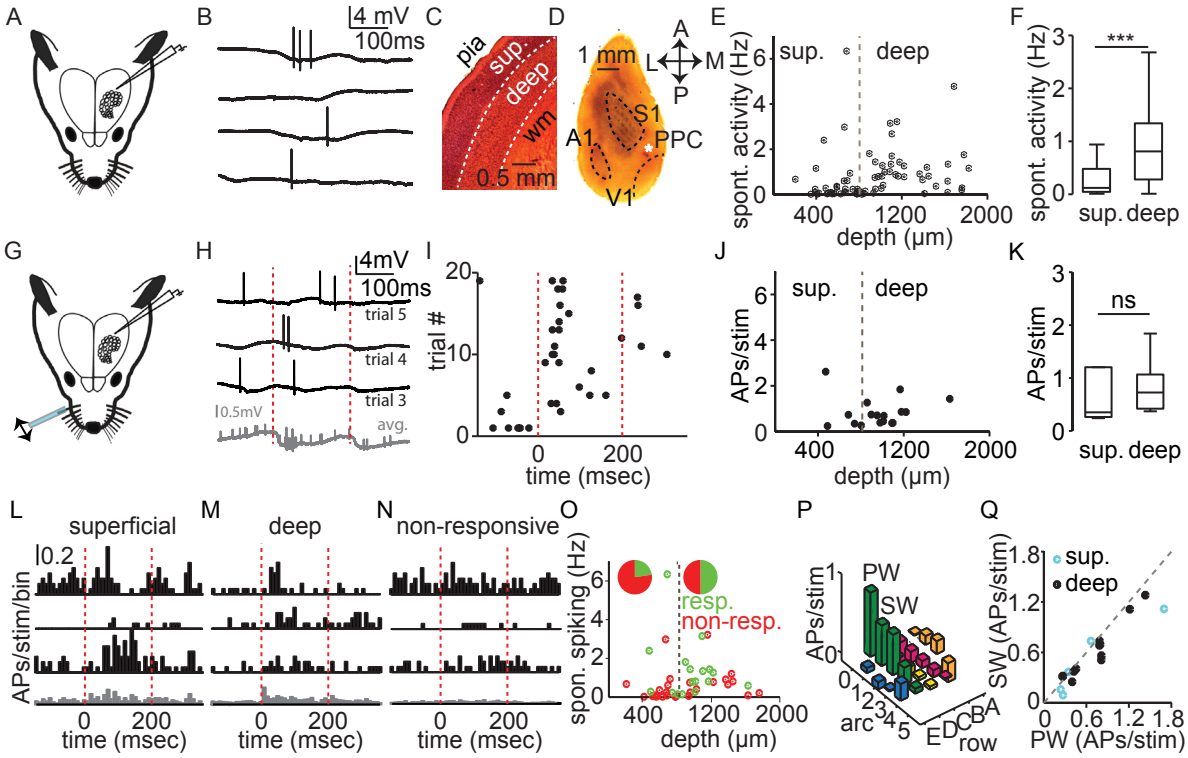

Figure 1. Properties of action potential response to passive whisker deflection in PPC. **A.** *Experimental design for juxtasomal recordings across layers of posterior parietal cortex (PPC) to quantify spontaneous activity.* **B.** *Example recording with snapshots of spontaneous activity of single PPC neuron.* **C.** *Coronal section through PPC in which Nissl staining reveals differences in cell body densities in PPC allowing the subclassification into superficial and deep layers (relatively high and low density, respectively).* **D.** *Tangential section of cortex including layer 4 of somatosensory cortex. Cytochrome C staining reveals anatomical landmarks to mark primary somatosensory (S1), primary visual (V1) and primary auditory cortex (A1).* **E.** *Spontaneous activity (in Hz) of individual neurons across recording depth in PPC. The bracket line indicates the border between superficial and deep compartments.* **F.** *Spontaneous activity is significantly higher in deep layers compared to superficial layers (Wilcoxon rank sum test, $p < 0.0001$, Superficial $n = 35$, Deep $n= 37$)* **G.** *Experimental design to record whisker-evoked activity across PPC layers.* **H.** *Example recording with action potential spiking during 3 consecutive whisker-stimulation trials (trial 3-5). The grey trace illustrates the average of 20 single whisker stimulation trials. Red bracket lines show on- and offset of whisker stimulation, respectively.* **I.** *Raster plot of experiment from panel H showing action potentials as individual bullets in response to 20 single whisker stimulation trials.* **J.** *Scatterplot to show the correlation between recording depth and evoked activity. Only individual units are shown in which spiking activity during whisker stimulation significantly exceeded spontaneous activity.* **K.** *Whisker-evoked activity is comparable between superficial and deep PPC layers (Wilcoxon rank sum test, $p = 0.23$, $n = 5$ for superficial, $n= 12$ for deep layers).* **L.** *Example peri-stimulus-time histograms (PSTHs) for individual units (in black) or average (in gray) for significantly activated units in superficial layers.* **M.** *Analogous to L but for deep layers.* **N**. *Example PSTHs for non-responsive neurons (see Methods for definition of non-responsive).* **O.** *Scatterplot to illustrate the fraction of neurons significantly responding to whisker stimulation as a function of recording depth and spontaneous activity. Pie charts show the fraction of response neurons in superficial and deep layers, respectively. These fractions are not significantly different (Fisher exact, $p = 0.07$, $n =5$ out of 22 for superficial, $n = 12$ out of 24 for deep layers, respectively).* **P.** *Example receptive field map for a single unit in PPC. The whisker evoked the largest response is labeled Principle Whisker (PW). The whisker generating the second largest response is considered the dominating Surround Whisker (SuW).* **Q.** *Scatterplot showing the ratio between PW and SuW response. Most units are close to the unity line (bracket line), indicative of low specificity of PW with respect to SuW.*

termined with intrinsic optical imaging (see Methods) and electrophysiological recordings targeted posterior to the S1 edge. Spontaneous action potential (AP) spiking activity was acquired (Fig.1A,B) and correlated to recording depth (Fig.1C-E). Only a subset of recorded neurons was sufficiently biocytin-labeled for full 3D morphological reconstruction, preventing a reliable cell-type specific analysis of spiking properties. However, the PPC can be subdivided into two cyto-architectural layers based on cell-body density, (border at ±850 µm from pia, Paxinos ATLAS). We found that spontaneous activity in deep layer was significantly higher compared to the superficial layer indicating layer-specific organizational principles (median 0.09 Hz, 1st/3rd Quartile = 0.04/0.35 Hz for superficial and median 0.88 Hz, 1st/3rd Quartile = 0.39/1.36 Hz for deep layers, respectively, Wilcoxon rank sum test p<0.0001).

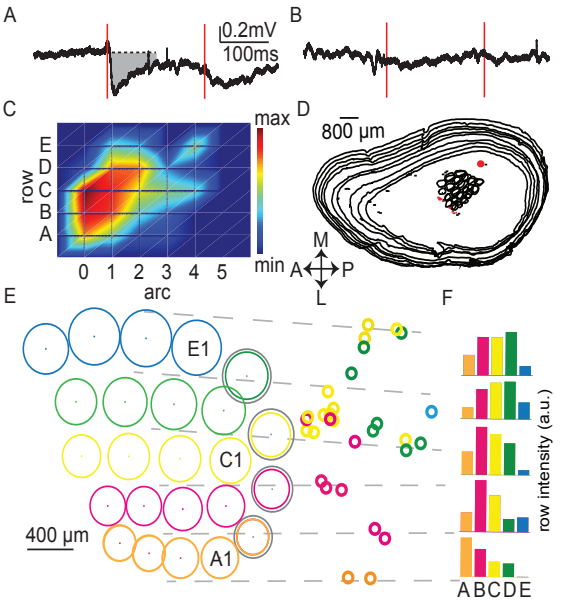

Figure 2. LFP receptive field mapping reveals functional somatotopy in PPC. **A.** *Example recording with average trace for twenty consecutive single whisker deflections showing the onset evoked local field potential response (LFP). Grey shaded area is the 0-100 post stimulus window used to quantify the single-whisker LFP intensity. Red lines indicate onset and offset for whisker deflection.* **B.** *Control condition with piezo in place but without whisker contact to illustrate the tactile nature of PPC-LFP after whisker deflection.* **C.** *Example LFP receptive field heat map for an individual PPC neuron showing LFP intensity across individual whiskers. Whisker row generating maximum average intensity was used to color code an individual recording site (see 2E).* **D.** *3 dimensional reconstruction of cortical sections in addition to barrel contours and position of recorded neuron.* **E.** *Recording locations projected onto standardized reference frame. Color code of recording location matches the color code of the whisker row that generated the maximum response.* **F.** *Bar plots illustrating the normalized mean LFP intensity per whisker row illustrating somatopy as a shift from dorsal (A-row) to ventral(E-row) whiskers along the medial-lateral axis.*

To determine the layer-specific organization of tactile stimulus-evoked activity, we quantified AP spiking in response to mechanical (passive) whisker deflection (Fig.1G, H). Individual whiskers were deflected 20 times and single-cell raster plots constructed (Fig.I). In a subset of recordings (n = 17 from total 37, Methods) and across layers, we found that whisker deflection significantly increased spiking activity indicative of PPC recruitment during passive somatosensory processing (Fig.1J). In superficial layers, the fraction of individual neurons significantly activated by whisker stimulation was 23% (n = 5 out of n = 22 superficial layer recordings). The fraction of neurons significantly activated upon whisker stimulation in deep layers was 50% (n = 12 out of n = 24 deep layer recordings). The layer-specific fraction of responsive neu-

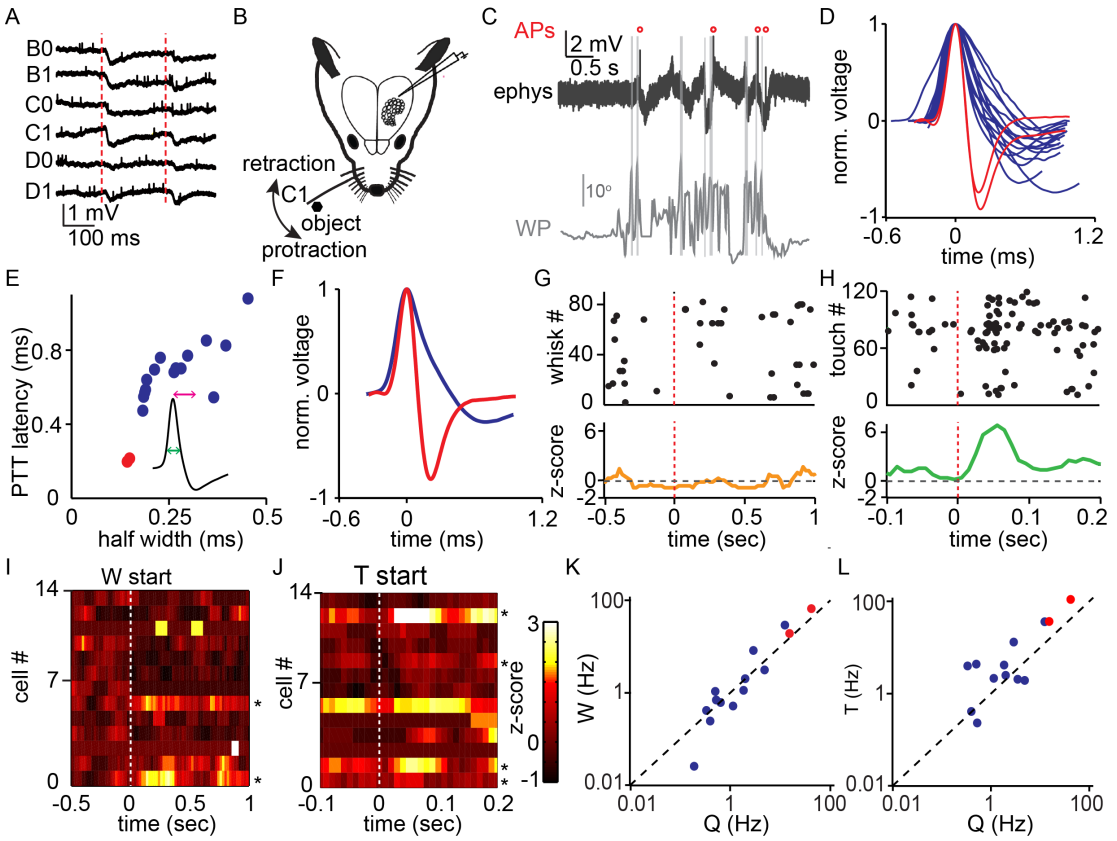

Figure 3. Single cells in PPC show AP responses during active whisking and object touch.

A. *Average LFP responses after 20 single whisker deflections for specific whiskers. Red bracket lines illustrate whisker stimulus on- and offset. Note that C1 whisker stimulation generated maximal LFP response.* **B.** *Experimental design for juxtasomal recordings across PPC layers in awake, behaving rats.* **C.** *Example segment of juxtasomal recording from individual PPC neuron. Red bullets illustrate occurrence of action potentials. In grey, whisker position obtained through high-speed-videography at 200Hz and offline tracking. Rectangle bars in grey highlight the occurrence of object touch, resulting from self-induced exploratory whisker motion.* **D.** *Average action potential waveforms of all juxtasomally recorded PPC neurons. Units with relatively narrow spike waveform are highlighted in red.* **E.** *Scatterplot of action potential half width and peak to trough latency for individual recordings. Green arrow indicates half width. Red arrow indicated peak to trough latency. Blue dots indicate putative pyramidal cells, (n=14) and red dots indicate putative interneurons (n=2) separated following unsupervised cluster analysis.* **F.** *Waveforms for putative pyramids and putative interneurons were averaged and normalized to peak.* **G.** *Rasterplot of individual recording from awake behaving rat in which spiking (individual bullets) is aligned to the onset of whisking. Bottom: normalized spiking (as z-score) aligned to onset of whisking. Note that in this unit, whisking was not accompanied by changes in spiking activity.* **H.** *Rasterplot of individual recording aligned to touch onset. Bottom: normalized spiking (as z-score) illustrates robust increase in spiking associated to whisker touch. Same recording as in G.* **I.** *Heat map of z transformed spiking rates for all putative pyramidal cells (n=14) triggered to whisking onset. Each row represents the spiking for a single recording. White line illustrates whisking onset. Units in which spiking activity significantly increased upon whisking are highlighted by an asterisk.* **J.** *Analogous to I, but spiking aligned to onset of active object touch. Units in which spiking activity significantly increased upon object touch are highlighted by an asterisk.* **K.** *Rasterplot illustrating the change in spiking activity upon free whisking (WO) with respect to quiescent (Q). Bracket line indicate unitary line.* **L.** *Analogous to K, but for spiking during object touch (T) versus quiescent epidodes(Q).*

rons was not significantly different for superficial vs deep layers (p=0.07, Fisher exact test), suggesting that both layers are equally involved in suprathreshold representation of whisker stimulation (Fig.1L-O). We almost exclusively found multi-whisker receptive fields in PPC recordings in which the ratio between principle whisker response (max response) and surround whisker was close to 1 (ratio = 0.83 ± 0.22 (mean ± std), n = 17). This could imply a receptive field transformation in the projections from S1 to PPC. The PW/SuW response ratios were comparable between layers (superficial ratio= 0.74 ± 0.31, deep ratio= 0.88 ± 0.18, Wilcoxon rank sum test p = 0.44). In conclusion, we found layer-specific spontaneous spiking activity in PPC, but suprathreshold representation of passive whisker stimulation is comparable between superficial and deep layers for 1) fraction of responsive neurons, 2) amplitude of response and 3) whisker specificity.

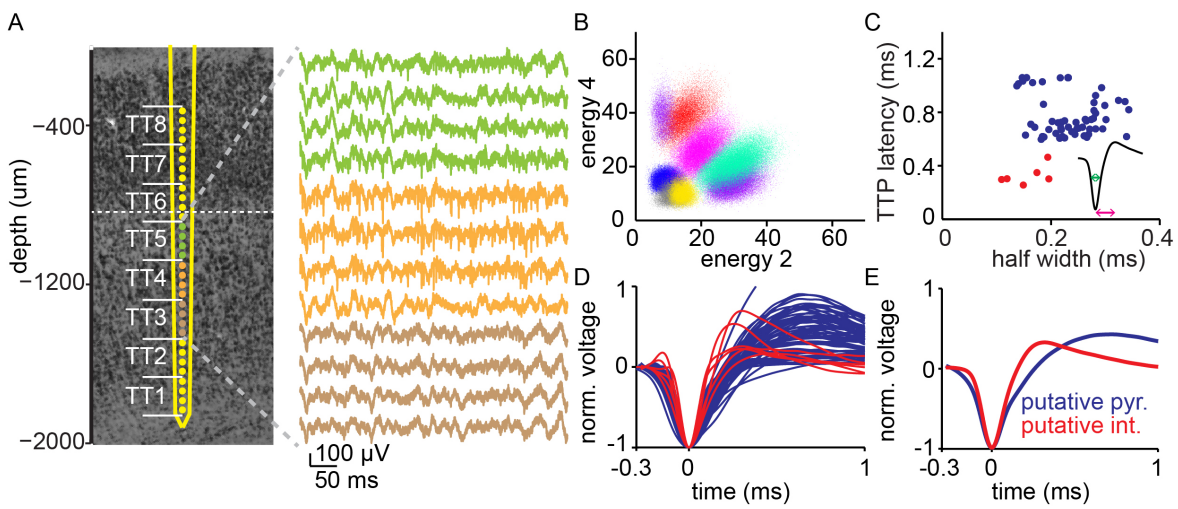

Figure 4. Silicon probe layout and spike clustering.
A. *Structural layout and positioning of the 32 channel silicon probe across PPC layers superimposed on a coronal section with Nissl stained cell-body densities. White solid lines indicate grouping of channels into tetrode configuration used for clustering putative units. This generated 8 tetrodes across all PPC layers. White bracket line indicates border between superficial and deep layers, respectively. Right: example traces illustrating activity recorded from each channel for 12 channels. Each color represents four channels from a single tetrode group.* **B.** *Eight putative units in different colors isolated from one tetrode configuration plotted against two of the dimensions used for clustering.* **C.** *Scatterplot of action potential half width and trough to peak latency for individual recordings. Green arrow indicates half width. Red arrow indicated through to peak latency. Blue dots indicate putative pyramidal cells, (n=102) and red dots indicate putative interneurons (n=11) separated following unsupervised cluster analysis.* **D.** *Average action potential waveforms of all recorded PPC neurons. Units with relatively narrow spike waveform are highlighted in red.* **E.** *Waveforms for putative pyramids and putative interneurons were averaged and normalized to trough.*

Presence of functional whisker somatotopy across PPC.

PPC and S1 are anatomically connected through reciprocal pathways (Lee *et al.* 2011; Oberlaender *et al.* 2011) and tactile stimulation evokes neuronal activity in the PPC visuotactile subregion (Olcese *et al.* 2013). It is unknown however, whether rat PPC has functional somatotopy, even though somatotopy is reliably present throughout the trigemino-thalamocortical pathway. To fill this gap in understanding PPC organization, we measured local field potential (LFP) intensity in the 0-100 ms after consecutive single whisker stimulations and correlated LFP intensity to whisker identity and recording location (Fig.2A-D). Whisker stimulation is represented consistently in LFP and LFP-receptive field maps were obtained for n = 31 recordings. Uopn whisker-clipping, PPC LFP responses to tactile stimulation were lost, indicating that LFP responses to whisker stimulation were specific for tactile input (Fig.2B). The whisker-evoked LFP intensity was quantified as the integral of the juxtasomal (extracellular) signal of the 0-100 ms post-stimulus window (Fig.2A). The receptive field map was obtained by subsequently deflecting different individual whiskers and computing the whisker-specific intensity (Fig.2C, Methods). To recover the recording location, neurons were biocytin-loaded and relevant anatomical landmarks were reconstructed to annotate receptive field maps to a standardized anatomical framework (Egger et al. (2012), Fig. 2D, E). The presence of somatotopy was revealed by calculating the mean LFP intensity for each whisker row and color-coding the recording location to the row generating maximum mean LFP intensity (Figure 2E, Methods). Barrel centers were used to spatially delineate areas of PPC corresponding to specific whisker barrel rows and average tuning values were determined for these 5 subdivisions of PPC. We found that the preferred whiskers shifted from the A-row from lateral recording positions to C/D-row whiskers when recording from medial locations (Fig.2F). Our recordings reveal for the first time functional somatotopy in PPC and this somatotopy most likely emerges from the structural somatotopy observed within S1-PPC projections (Lee *et al.* 2011).

Individual PPC neurons represent self-induced whisker motion and object touch

Since we observed whisker-evoked activity in PPC of anaesthetized rats, the next question we addressed is whether self-induced (voluntary) whisking and object touch is encoded in PPC of awake, behaving rats (Fig.3). We juxtasomally recorded single units in PPC during voluntary, self-induced active tactile exploration (see Methods). During the initial phase of the recording, rats were isoflurane anaesthetized to perform RF mapping and to identify the whisker generating the maximal LFP intensity (Fig.3A). The principle whisker (PW) was spared and remaining surround whiskers (SuWs) clipped after which the isoflurane anaesthesia was terminated (Fig.3B). Rats would quickly wake up and rats initiated whisker movements. The presence of an object within reach of the

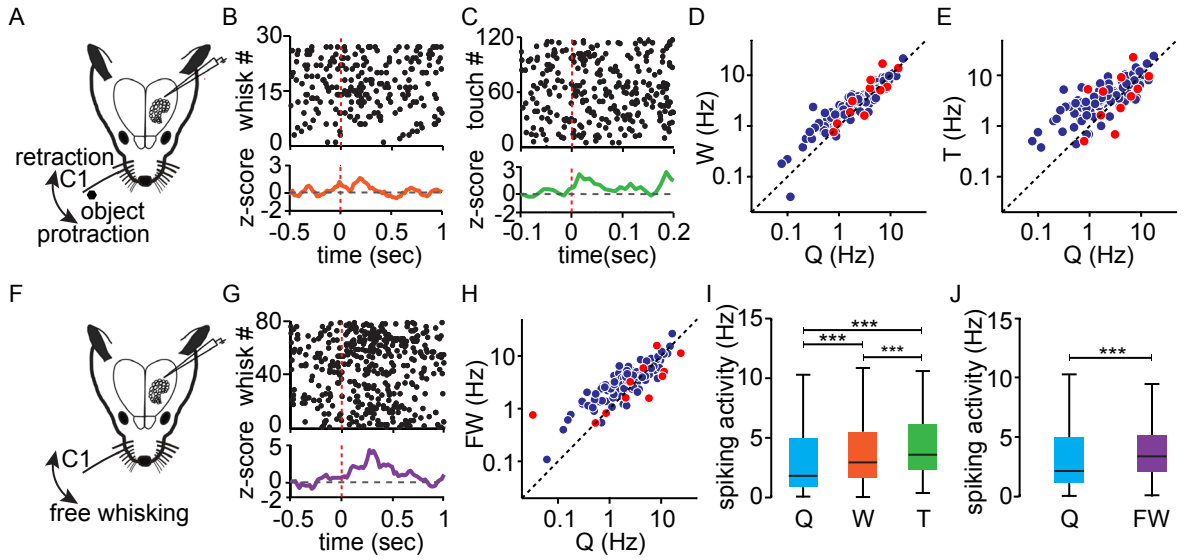

Figure 5. PPC encodes whisker motion and whisker touch.
A. *Experimental design for silicon probe recordings across layers of posterior parietal cortex (PPC) to quantify the correlation between whisking and PPC spiking activity. Whisking episodes are behavioral windows in which whiskers were in motion, but not in contact with the object.* **B.** *Raster plot of an example single unit from silicon probe recordings aligned to onset of whisking. Black dots represent individual action potentials. Lower panel: z transformed spiking activity aligned to whisking onset.* **C.** *Raster plot of the same unit triggered to onset of object touch. Lower panel: z transformed spiking activity aligned to touch onset.* **D.** *Population statistics to illustrate the significant increase of PPC spiking upon whisking onset (Wilcoxon signed rank test, $p < 0.0001$, $n = 113$). Blue bullets represent putative pyramids and red bullet represent putative inhibitory neurons, respectively.* **E.** *Analogous to D, but for comparison of spiking activity during quiescent versus touch episodes.* **F.** *Experimental design for silicon probe recordings across PPC layers to quantify the correlation between exploratory –free- whisking and PPC spiking activity (object was not present).* **G.** *Raster plot of an example single unit from silicon probe recordings aligned to onset of free whisking. Black dots represent individual action potentials. Lower panel: z transformed spiking activity aligned to whisking onset.* **H.** *Analogous to D and E, but for quiescent episodes versus free whisking episodes. Spiking significantly increased during free whisking (Wilcoxon signed rank test, $p < 0.0001$, $n = 113$).* **I.** *Boxplots illustrating the collapsed population statistics for spiking activity during quiescent, whisking and touch episodes, respectively. Note that both whisking and object touch significantly increase spiking activity in PPC (Wilcoxon signed rank test, $p < 0.0001$, $n = 113$ units).* **J.** *Spiking activity in PPC is significantly increased during free whisking (no object present, Wilcoxon signed rank test, $p < 0.0001$, $n = 113$ units).*

whiskers induced self-induced whisker contact with the object (active touch) (Fig.3B). We recorded AP spiking activity using juxtasomal recordings in addition to high speed videography (200Hz) to track whisker position and object touch (Fig.3C). Across recordings we obtained 1023 touch events, with median duration of 40 ms (1st/3rd Quartile 25/80 ms), with intertouch interval of 135 ms (1st/3rd Quartile 70/1193 ms). In a subset of experiments, recorded neurons were biocytin-loaded for post-hoc morphological reconstructions (Egger *et al.* 2012; Narayanan *et al.* 2014). Alternatively, the recording location was labeled with an extracellular biocytin deposit (Moore, Deschenes, et al. 2015). Juxtasomally recorded neurons were targeted predominantly to the deeper lay-

ers due to the relatively high fraction of whisker-stimulus responsive neurons in deep layers (Fig.2). We subclassified recorded neurons based on AP waveforms into putative excitatory neurons (RSU, regular spiking neurons) and putative interneurons (FSU, fast spiking interneurons). Neurons with relatively short half width and peak-to-trough (PTT) latency were classified as putative interneurons (red) and neurons with relatively broad half width and PTT latency as putative excitatory neurons (blue) (Bartho et al. 2004)(Fig.3D-F).

To determine whether spiking activity of individual PPC neurons in awake behaving rats correlate with different sources of somatosensation such as efferent copy and ex-afference information (Ahissar et al. 2000; Diamond *et al.* 2008; Moore, Mercer Lindsay, *et al.* 2015), we categorized behavior into episodes of quiescence (Q), whisking (W) and object touch (T) and quantified state-dependent spiking activity. Whisking (W) period consisted of episodes with whisker movements without object contact. The whisking episodes carry efferent copy information, whereas touch events consist of both efferent copy and ex-afference information. Individual units showed heterogeneous responses to whisking or touch and a subset of neurons showed robust increases in spiking activity during W or T episodes (RSUs: W 2 out of 14, T 4 out of 14 (Fig.3G-J), FSUs W 1 out of 2, T 2 out of 2, not shown). Thus, modulation of spiking activity during whisking

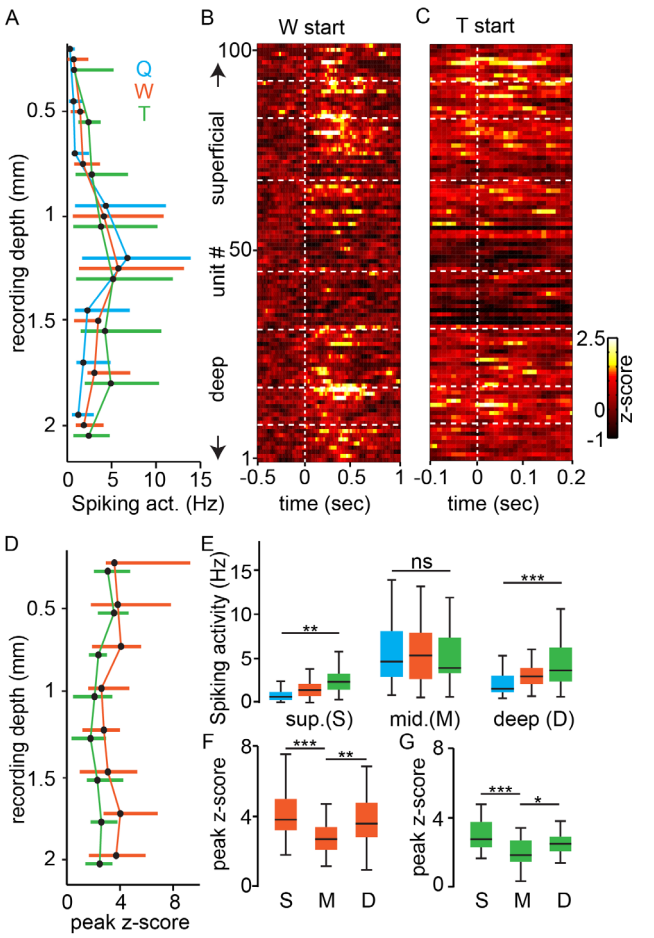

Figure 6. Layer-specific encoding of efferent copy and ex-afference information in PPC

A. *Spiking activity as a function of recording depth (250 µm bins) and across behavioral states (Quiescent, Whisking, Touch). Data is represented as median activity and 99 % of units recorded at the specific location.* **B.** *Heat map of z transformed spiking activity of all putative pyramidal units across recording depths in PPC aligned to whisking onset. Each row represents a single unit, which are arranged according to recording depth. White bracket lines indicate borders between tetrode groups.* **C.** *Analogous to B. but z-score transformed spiking activity is aligned to onset of object touch. Note that in panel B and C, changes in spiking upon whisking onset or object touch is observed in superficial and deep layers, but not in middle layers.* **D.** *Peak z-scores to indicate maximal changes in spiking activity as a function of recording depth (250 µm bins) and for Whisking (orange) and Touch (green). Note that peak z-scores are relatively low in middle layers, indicative of lack of response to Whisking or Touch* **E.** *Box plots illustrating population statistics for encoding efferent copy (whisking) or ex-afference (object touch). Whisking and Touch are significantly represented*

in superficial and deep layers (Putative pyramidal units, Wilcoxon signed rank test, p < 0.0001 , n = 33 for superficial and n = 33 for deep layers, respectively. In middle layers, spiking activity is not modulated by whisking or touch (Wilcoxon signed rank test, p > 0.05, n = 36). **F.** *Box plots with population statistics for peak z-scores across layers in the 0-1 second after Whisking onset. Peak z-scores were significantly higher in superficial and deep layers compared to middle layers (Wilcoxon rank sum test, p < 0.01, superficial n = 33, deep n=33, middle n=36).* **G.** *Analogous to F but for peak z-scores in the 0-100 ms after touch onset. Peak z-scores were significantly higher in superficial and deep layers compared to middle layers (Wilcoxon rank sum test, p < 0.05, superficial n=33, deep n=33, middle n=36)*

or touch was observed robustly in a small fraction of the recordings, consistent with coding principles in S1 where a small fraction of the neuronal population is responsible for sensory representation (O'Connor et al. 2010). In 2 out of 16 recordings we found significant modulation from Q to W and from W to T, which could reflect integrative properties of these neurons of both efferent copy and ex-afferent information during active tactile sensation.

On the population level, we also found behavior-dependent spiking in PPC with increased spiking during whisking (efferent copy) and object touch (ex-afference)(Fig.3K, L) (mean + stdev spiking rate for n=14 RSU: Q = 2.31 ± 3.20 Hz, W = 3.37 ± 7.71 Hz, T = 5.07 ± 9.56 Hz; Q vs W p = 0.66, Q vs T p = 0.29, W vs T p = 0.03, Wilcoxon signed rank test, mean spiking rate for n=2 FSUs Q = 28.45 ± 18.58 Hz, W = 42.76 ± 33.31 Hz, T = 73.19. ± 51.65 Hz). An alternative method to quantify state-dependent spiking is

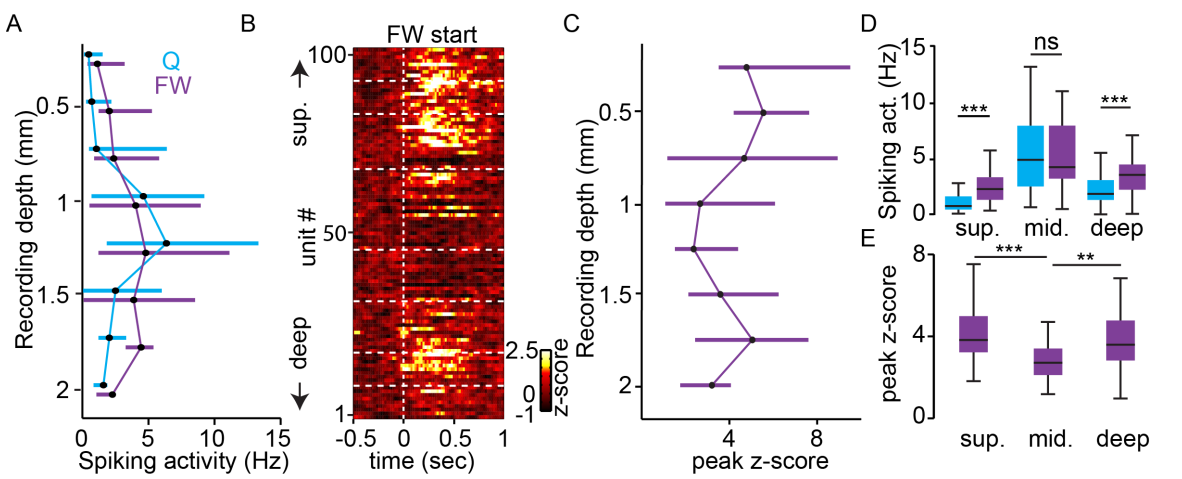

Figure 7. Efferent-copy encoding in PPC during free whisking.
A. *Spiking activity as a function of recording depth (250 µm bins) and across behavioral states (Quiescent, Free Whisking). Data is represented as median activity and 99 % of units recorded at the specific location.* **B.** *Heat map of z transformed spiking activity of all putative pyramidal units across recording depths in PPC aligned to onset of free whisking. Each row represents a single unit, arranged according to recording depth. White bracket lines indicate borders between tetrode groups.* **C.** *Peak z-scores to indicate maximal changes in spiking activity as a function of recording depth (250 µm bins) for the 0-1 sec window after onset of free whisking. Note that peak z-scores are relatively low in middle layers, indicative of lack of response to onset of Free Whisking.* **D.** *Box plots illustrating population statistics for encoding efferent copy (free whisking) across PPC layers. Free whisking is significantly represented in superficial and deep layers (Statistics, p< 0.0001, n = 33 for superficial and deep layers, respectively, Wilcoxon*

signed rank test). In middle layers, spiking activity is not modulated by free whisking (p = 0.96, n = 36, Wilcoxon signed rank test). **F.** *Box plots with population statistics for peak z-scores across layers in the 0-1 second after Whisking onset. Peak z-scores were significantly higher in superficial and deep layers compared to middle layers (Wilcoxon rank sum test, p < 0.001, superficial n=33, deep n=33, middle n=36).*

to compute the variability in the PPC population during W and T episodes relative to Q episodes using the population mean squared error (mse) (distance to unity for individual units, Fig. 3K,L). The mse was significantly higher for Q versus T compared to Q versus W (mse Q vs. W=59.60 ± 162.64 versus mse Q vs. T= 363.28 ± 1153.20, p=0.0034, Wilcoxon signed rank test) indicating a larger effect of object touch on PPC spiking compared to the effect of whisking on PPC spiking.

Ensemble recordings reveal increased population activity during sensorimotor processing in PPC

Single-unit juxtasomal recordings provide unprecedented insight into coding mechanisms for individual neurons, but it does not allow studying population activity or distributed population coding. To study ensemble coding of sensorimotor behavior in PPC, we used 32 channel linear silicon probes to obtain population activity across PPC layers of awake behaving rats again during self-generated whisking and object touch (Fig.4A, see Methods). Multi-unit data was spike-sorted with MClust (A. David Redish, University of Minnesota, USA) using a tetrode configuration (Reyes-Puerta et al. 2015) and average spike waveforms for individual clusters were used to categorize individual units into putative excitatory neurons (RSUs, n = 102) and putative interneurons (FSUs, n = 11) (Fig.4C-E, see Methods). Ensemble activity was recorded and spiking data for single unit correlated to episodes of Q, W and T. Also in the ensemble recordings, we found evidence for single unit representation of whisking (W) and object touch (T) (Fig.5A-C). To compare variation in spiking activity during quiescent (Q), whisking (W) and object touch (T) episodes, we quantified spiking rates for all units during whisking (W) and touch (T) to Quiescent (Q),Fig 5D,E) and compared mse for both conditions . The variation in spiking activity was significantly larger during object touch (T) compared to whisking (W) (mse Q vs. T 8.75 ± 24.97 versus mse Q vs W 2.43 ± 9.47, p<0.0001, Wilcoxon signed rank test). We next quantified population spiking activity across the three behavioral conditions and found a significant increase in spiking activity during whisking compared to quiescent (median Q 1.81 $1^{st}/3^{rd}$ Quartile = 0.87/4.95 Hz < median W 2.94 Hz Quartile $1^{st}/3^{rd}$ = 1.67/5.51 Hz, p < 0.0001 Wilcoxon signed rank test, Fig.5I) Also during whisker touch, the spiking activity for PPC units is significantly higher compared to whisking episodes median W 2.94 Hz Quartile $1^{st}/3^{rd}$ = 1.67/5.51 Hz < median T 3.58 Hz Quartile $1^{st}/3^{rd}$ = 2.32/6.13 Hz, p<0.0001, Wilcoxon signed rank test Fig.5I). The largest difference in spiking activity was found when comparing quiescent versus

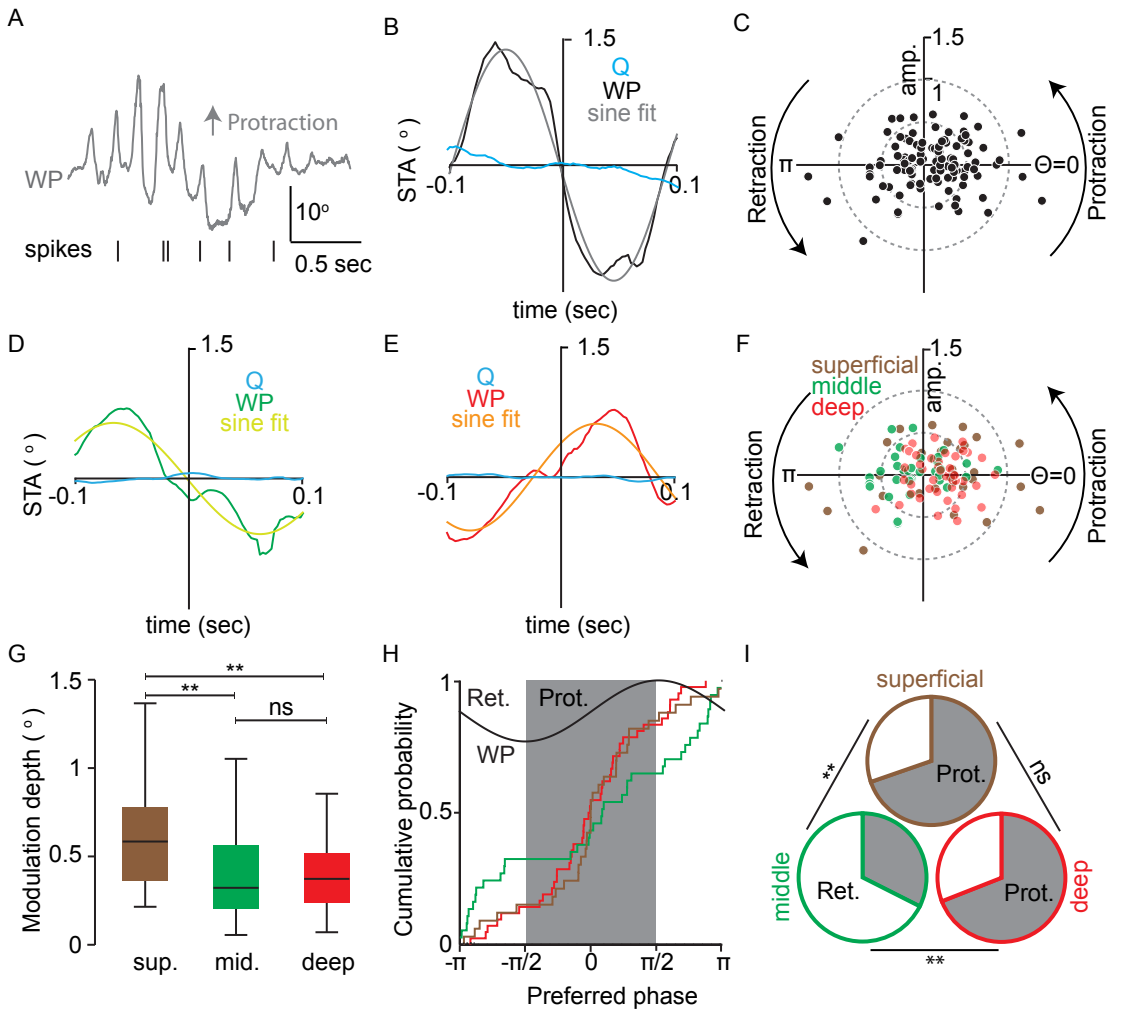

Figure 8. Layer specific tuning to whisking phase information in PPC.
A. *Example snapshot of raw data illustrating spiking activity during whisking (WP = whisker position in degrees).* **B.** *Spike triggered-average (STA) of whisker position during quiescent (blue) and whisking (black) episodes for unit shown in A. In grey the sine fit to the STA to extract preferred phase and modulation depth.* **C.** *Scatter plot illustrating the modulation depth versus phase for individual units. Protraction is covered by the 0 – 0.5π and 1.5π - 2 π quadrants with maximum protraction at 0.5 π. Retraction is covered by the 0.5 – 1.5 π with maximum retraction at 1.5 π.* **D.** *Spike triggered-average (STA) of whisker position during quiescent (blue) and whisking (black) episodes for one example unit from the middle layer. In light green the sine fit to the STA to extract preferred phase and modulation depth. Note that this example neuron preferentially spikes during retraction.* **E.** *Analogous to D but for one example unit from the deep layer. Note that this example neuron preferentially spikes during protraction.* **F.** *Scatter plot illustrating the modulation depth versus phase for individual units as a function of recording depth.* **G.** *Modulation depth is significantly higher in superficial layers compared to middle and deep layers (Wilcoxon rank sum test, p < 0.005, n = 30 , n= 35, n = 42 for superficial, middle and deep layers, respectively).* **H.** *Cumulative histogram illustrating the preferred phase extracted from the STA as a function of recording depth. The grey shaded area represents the protraction phase of the whisker cycle, the white area represents the retraction phase, respectively. Note that the superficial (brown) and deep (red) units are tuned preferentially to whisker protraction.* **I.** *Pie charts illustrating the layer-specific fraction of units tuned to protraction versus retraction. In superficial layers, 70 % of units is tuned to whisker protraction, which is comparable to the 69 % tuned to protraction in deep layers (Fisher exact, p = 1) but significantly different compared to middle layers where only a minor fraction of units is tuned to protraction (32 %, Fisher exact, S vs. M p = 0.003, D vs. M p = 0.002) and most units are tuned to retraction (68%).*

touch (median Q 1.81 1st/3rd Quartile = 0.87/4.95 Hz < median T 3.58 Hz Quartile 1st/3rd = 2.32/6.13 Hz, p<0.0001, Wilcoxon signed rank test Fig.5I). Using both juxtasomal single-unit (n = 16) and silicon probe ensemble recordings (n = 113) we conclude that whisking and object touch (efferent copy + ex-afference) are significantly represented in spiking activity in PPC.

Since PPC is involved in coding for movement intention and action plans (Andersen 1997; Andersen *et al.* 1997; Snyder *et al.* 1997, 1998; Andersen and Cui 2009), we next wanted to study how efferent copy information is represented under conditions of unrestricted exploratory whisking (no object present, free whisking (FW), Fig.5F). Also during free whisking, we found that spiking activity significantly increased for individual units compared to quiescent episodes (Fig.5G). This was confirmed using population statistics where we found a significantly higher spiking activity during free whisking compared to quiescent episodes (median and 1st/3rd Quartile median Q 2.14 Hz Quartile 1st/3rd = 1.15/4.95 Hz < median FW 3.37 Hz Quantile 1st/3rd = 2.06/5.10 Hz, Wilcoxon signed rank test, p < 0.0001, Fig.5H,J). Our single unit and ensemble recordings during 2 types of whisking behavior (whisking with object versus free whisking) unambiguously show that efferent copy information is represented within the PPC circuitry and leading to increased PPC spiking activity. Additionally, object touch (ex-afference information) further increases spiking activity, implying that efferent copy and ex-afferent information is merged within the PPC microcircuit. Similarly to juxtasomal recordings, we found significant modulation in 12 % of units (13 out of 113 units) from Q to FW and from W to T, which could reflect integrative properties of these neurons of both efferent copy and ex-afferent information during active tactile sensation.

Layer specific sensorimotor processing in PPC

A canonical organization has been suggested for neuronal circuits across cortical areas and the organizational principles include cell-type and layer-specific functions during sensorimotor processing or cognitive performance. We therefore determined whether we could find evidence for layer-specific correlations between PPC spiking activity and sensorimotor behavior. Silicon probe recordings with a linear channel layout across layers allows to link a specific recording depth to high-quality clusters during the single unit cluster analysis. We quantified spiking activity for individual tetrode groups along the span of PPC layers (with 250 µm bins) and correlated the average spiking activity to the three different behavioral states (Q, W, T)(Fig.6A). We found a layer-specific profile for spontaneous activity, similar to cell-type and layer-specific spiking activity in sensory cortices (de Kock *et al.* 2007; de Kock and Sakmann 2009; Sakata and Harris 2009).

Based on the spontaneous activity profile (Quiescent episodes), we further subdivided the PPC layers into three compartments; superficial (300-850 μm), middle (900-1250

μm) and deep layers (1300-1850 μm). To quantify the magnitude of changes in spiking activity as well as the temporal aspects of behavior-dependent activity modulation of single unit, we constructed heat maps of the (z-transformed) spiking activity. Spiking activity of putative excitatory units were aligned to either whisking onset or object touch while preserving the recording depth of individual units in the heat maps (Figure 6B,C). For whisking (W), we found that putative excitatory units in superficial and deep layers responded with an increase in spiking activity (Fig.6B,C). Single units recorded in the middle layer did not show the correlation between whisking and increased spiking activity. Similarly, we found increased spiking activity upon touch in superficial and deep PPC layers, but no correlation between whisking and changes in spiking activity in the middle layer (Fig.6C).

To quantify the behavior-dependent change in spiking activity, we extracted peak z-scores from the heat maps for each unit and binned these values according to recording depth (200 µm bins, Fig.6D). Units recorded in superficial and deep layers showed relatively high peak z-scores during both whisking (W) and object touch (T) behavior compared to units in the middle layer. Population statistics on either absolute spiking activity (in Hz) or behavior-dependent modulation of spiking activity (z scores) revealed multiple layer-specific functions in PPC during whisking and touch (Fig.6E-G). First, whisking and object touch significantly increased spiking frequency in superficial layers compared to spiking during quiescent (median and 1st/3rd Quartile RSU; median Q 0.69 Hz 1st/3rd Quartile = 0.33/1.23 Hz < median W 1.46 Hz 1st/3rd Quartile = 0.78/2.16 < median T 2.39 Hz 1st/3rd Quartile = 1.50/3.30 Hz, n = 33, $p < 0.001$ for all comparisons, Wilcoxon signed rank test). Similarly, whisking and object touch also significantly increased spiking frequency in deep layers (median Q 1.60 Hz 1st/3rd Quartile = 1.20/3.06 Hz < median W 2.98 Hz 1st/3rd Quartile = 2.12/3.94 Hz < median T 3.67 Hz 1st/3rd Quartile = 2.44/6.24 Hz, n = 33, $p < 0.0001$ for all comparisons, Wilcoxon signed rank test). Units in the middle layers did not show a significant change in spiking activity during whisking (W) or object touch (T) compared to quiescent periods (median Q 4.67 Hz 1st/3rd Quartile 2.94/8.10 Hz, median W 5.35 Hz 1st/3rd Quartile = 2.71/7.90 Hz, median T 3.93 1st/3rd Quartile = 3.38/7.39 Hz, n = 36, $p > 0.05$ for all comparisons, Wilcoxon signed rank test). Thus, efferent copy and ex-afference information are represented by increased spiking activity in superficial and deep layers but not middle layers of PPC. To rule out the influence of differences in layer-specific spontaneous activity on population statistics, we compared absolute spiking frequencies as z-scores. Also for z-scores, we found significant changes in spiking activity during whisking and object touch, with significantly higher peak z scores in superficial and deep layers compared to middle layers (median W superficial 3.82 1st/3rd Quartile = 3.22/4.99 > median W middle 2.71 1st/3rd Quartile = 2.11/3.40 , $p<0.0001$; W middle 2.71 1st/3rd Quartile = 2.11/3.40 < median W deep 3.59 1st/3rd Quartile = 2.82/4.77, $p = 0.001$; median T 2.76 superficial 1st/3rd Quar-

tile = 2.30/3.75 > median T middle 1.84 1st/3rd Quartile = 1.48/2.69, p = 0.0001; median T middle 1.84 1st/3rd Quartile = 1.48/2.69 < median T 2.50 deep 1st/3rd Quartile = 2.06/2.91, p = 0.01, Wilcoxon rank sum test; superficial n=33, middle n = 36, deep n = 33, Fig.6F, G). Ensemble recordings in PPC layers therefore uncovered layer-specific coding of efferent copy and ex-afference information.

The previous analysis revealed layer-specific representation of whisker motion in PPC. However, the object was within reach during whisker motion and therefore spiking during these episodes of whisking could also involve an expectancy or preparatory signal for object touch (Fox et al. 2003). To determine PPC activity during free exploratory whisking in air (FW), we repeated the experiment without the object present. Figure 7A shows the distribution of spiking activities versus recording depth during quiescent (Q) and free whisking (FW). We found similar layer-specific activity profiles (Fig.7A), z-score based heat maps (Fig.7B) and peak z-scores (Fig.7C) compared to Fig.6. Population statistics for spiking activity (RSU; median Q superficial 0.81 Hz 1st/3rd Quartile = 0.50/1.54 Hz < median FW superficial 2.33 Hz 1st/3rd Quartile = 1.37/3.20 Hz, p<0.0001; median Q deep 1.90 Hz 1st/3rd Quartile = 1.22/3.15 Hz < median FW deep 3.36 Hz 1st/3rd Quartile = 2.20/4.67 Hz, p<0.0001; median Q middle 4.95 Hz 1st/3rd Quartile = 2.75/7.95 Hz, median FW middle 4.29 Hz 1st/3rd Quartile = 3.17/7.98 Hz, p=0.96, Wilcoxon signed rank test , Fig.7D) and peak z-scores (median FW superficial 4.78 1st/3rd Quartile = 4.19/5.92 < median FW middle 2.52 1st/3rd Quartile = 1.84/3.10 , p < 0.0001; < median FW middle 2.52 1st/3rd Quartile = 1.84/3.10 < median FW deep 3.67 1st/3rd Quartile = 2.71/4.49, p < 0.001, Wilcoxon rank sum test ,Fig.7E). We conclude that superficial and deep layers but not middle layers encode whisker motion with increased spiking activity.

Layer specific encoding of whisker phase in PPC

To study whether PPC units encode whisker phase information (protraction vs retraction) (Diamond *et al.* 2008), we first computed spike triggered average (STA) for whisker angle during free whisking (FW) episodes versus quiescent episodes (Q, Fig.8A,B, de Kock and Sakmann (2009)). The STA was used to fit a sinusoidal curve to extract the preferred phase of whisking and degree of modulation (maximum amplitude of fitted sine curve, Fig.8B). The population polar plot indicates that all whisker phases are represented in the n = 112 recorded units with relatively large heterogeneity for modulation strength (Fig.8C). Next, we determined whether phase tuning showed layer-specific organizational principles, comparable to the layer-specific representation of whisker motion presented in Figs.6-7. We found that units in superficial layers were mainly tuned to protraction (n = 23 out of n=33. Fig.8D-I). Spiking in units from middle layers was preferentially tuned to retraction (n = 25 out of n = 37) and spiking in deep layers was again tuned to protraction (n = 29 out of n = 42), comparable to superficial layers (Superficial

– Middle, Fisher exact, $p < 0.005$, Middle – Deep, Fisher exact, $p < 0.005$). Thus, in addition to layer-specific increases in spiking activity induced by whisker motion, we find that whisker phase follows the same organizational principles: superficial and deep layers are both tuned to whisker protraction, resulting in increased spiking during whisker motion. Remarkably, even though middle layers do not show increased spiking activity correlated to whisker motion, spiking in middle layer units is preferentially tuned to whisker retraction (Fig.8H). In summary, during active whisking, superficial and deep layers in PPC increase activity and encode whisker protraction (efferent copy information). The middle layer does not show changes in spiking activity during whisking, but spiking is tuned to whisker retraction (efferent copy information). When whisker motion results in object touch, superficial and deep layers represent ex-afferent information, which is absent in the middle layer.

Discussion

The PPC is involved in a broad repertoire of cognitive behaviors including multisensory integration (Andersen 1997; Andersen *et al.* 1997; Avillac et al. 2007; Olcese *et al.* 2013). Here, we studied processing of isolated tactile information in rat PPC to understand the contribution of PPC to whisker-based somatosensation. We present three major findings: 1) PPC shows functional somatotopy along the medial-lateral axis, resembling the anatomical organization of the whisker pad and somatotopy throughout the trigeminothalamocortical pathway, 2) PPC encodes efferent-copy information in awake behaving rats via layer-specific increased action potential spiking and layer-specific representation of whisker protraction and whisker retraction, and finally 3) ex-afferent information (object touch) in awake behaving rats is encoded by individual units in superficial and deep PPC layers.

The posterior parietal cortex (PPC) has attracted relatively little attention when studying tactile sensation even though PPC has reciprocal connections with S1 (Lee *et al.* 2011; Wang *et al.* 2012) and vibrissal motor cortex M2 (Wang *et al.* 2012). This suggests that PPC could be a critical hub in the whisker sensorimotor circuitry where incoming somatosensory information is coupled to motor output. This is supported by recent anatomical evidence showing that PPC-projecting neurons in S1 are preferentially located in septal regions (Lee *et al.* 2011). These S1-septal regions are part of the paralemniscal pathway (Alloway 2008), which was suggested to specifically carry information on whisker motion (Ahissar *et al.* 2000; Yu et al. 2006; Alloway 2008). Recent evidence however challenged the idea that information on whisker touch and whisker motion is segregated in lemniscal/paralemniscal pathways. As a consequence, efferent-copy information could therefore be more commonly represented throughout the S1 microcircuit than previously thought (Moore, Mercer Lindsay*, et al.* 2015; Urbain et al. 2015).

An alternative pathway for conveying information on whisker motion to PPC could be the projection from S1-L5A pyramids which preferentially encode whisker self-motion (de Kock and Sakmann 2009) and a subset of these neurons have direct S1-PPC projections (Oberlaender *et al.* 2011). Since PPC receives little input from somatosensory thalamic nuclei (Lee *et al.* 2011), it is possible that the leminiscal and paralemniscal pathways contribute to encoding whisker self-motion in PPC. One potential strategy to uncover the causal relationship and detailed coding principles in PPC would be to selectively manipulate spiking activity of S1 neurons during whisking to determine the consequence on PPC representation of whisker protraction and retraction.

Importantly, we show that PPC is organized somatotopically indicating that tactile processing of individual whiskers occurs in dedicated functional zones, a well-known property throughout the whisker sensorimotor pathway and most obvious in primary somatosensory (barrel) cortex (Woolsey and Van der Loos 1970; Wimmer et al. 2010). The functional somatotopy we found in LFP signals matches the organizational principles of the S1-PPC feed-forward anatomical projections revealed using anterograde tracer injections (Lee *et al.* 2011). It will be interesting to determine layer-specific differences in organization of somatotopy or cell-type specific receptive field structure (de Kock *et al.* 2007), which was beyond the scope of the present study.

The PPC is primarily involved in complex cognitive behavior including decision-making, planning, and integration of multi-modal sensory information (Harvey *et al.* 2012; Olcese *et al.* 2013). This motivated us to investigate the contribution of PPC to processing of sensorimotor information under conditions of awake, natural behavior including whisker self-motion and whisker touch. During self-induced whisker motion, we found an unexpected laminar organization in PPC where superficial and deep layers encoded whisker motion with increased spiking and with preferred tuning to whisker protraction (Fig.5-8). In Contrast, middle layers did not show the increased spiking activity upon whisking with spiking preferentially tuned to whisker retraction. This layer-specific organization is very robust, since we found similar results during pre-touch whisking or when the object was not present and whisking involved exploratory free whisking in air. Assuming a canonical columnar organization in PPC, (Mountcastle 1997), activity could be oscillating between superficial/deep and middle layers during whisker protraction and whisker retraction. This could well be an efficient mechanism to encode and integrate whisker phase information to build whisker dependent reference frames (Curtis and Kleinfeld 2009). Furthermore, PPC function and layer-specificity of whisker phase representation need to be investigated under conditions of multisensory processing when tactile information is supplemented by information from additional sensory modalities (e.g. auditory or visual) to obtain a comprehensive perspective.

Compared to efferent copy coding, we observed comparable layer-specific organiza-

tional principles for PPC upon whisker touch (Fig.6) since the ex-afference signal increased spiking in superficial and deep, but not middle layers. This reflects layer-specific input pathways to PPC where middle layers receive different afferent input compared to superficial/deep layers. With new tools emerging such as rabies virus-based input mapping to reveal synaptically connected circuits with cellular resolution (Velez-Fort et al. 2014), it will be highly informative to determine the layer-specific presynaptic partners in PPC and formulate new working hypothesis on PPC in- and output transformations.

To conclude, we uncovered somatotopy in PPC and show layer-specific tactile processing in PPC of awake, behaving rats. This opens the path to design additional experiments to reveal cell-type specific contributions to sensorimotor processing. When this involves PPC, S1 and vibrissal M2, and perhaps even additional association areas, the sensorimotor loop can be closed to advance the coding and decoding algorithms of neuronal circuits underlying sensory-guided motor output. The advance of these algorithms will in turn push the development of neuro-prosthetics applications with sensorimotor function (Bensmaia and Miller 2014; Aflalo et al. 2015).

Materials and Method

Anaesthetize animal preparation

All experiments were carried out in accordance with the animal welfare guidelines of the VU University Amsterdam, the Netherlands. Urethane anaesthetized (1.6-1.7 g kg^{-1}) male Wistar rats (Harlan, 28-42 days post-natal, n=36) were used for in-vivo juxtasomal recording in posterior parietal cortex (PPC). Depth of anesthesia was checked by foot and eyelid reflex. The animal's temperature was monitored and maintained at 37^{o}C using a rectal probe and a thermostatically controlled heating pad during surgery and experiment. For passive whisker stimulation, all whiskers contralateral to the recording hemisphere were trimmed to 5 mm with respect to the whisker follicle. The posterior edge of the barrel cortex was identified using intrinsic optical imaging (de Kock *et al.* 2007) through deflection of individual straddler whiskers (D0, C0) using a glass capillary attached to a piezo electric bimorph. The cortical strip posterior to this, confined within the medial and lateral boundaries of S1, was described as PPC before (Kolb and Walkey 1987; Reep *et al.* 1994; Lee *et al.* 2011; Olsen and Witter 2016) and targeted as the recording site.

Juxtasomal recording and receptive field mapping

In vivo juxtasomal recording were made as previously described in (de Kock *et al.* 2007; Narayanan *et al.* 2014). Briefly, borosilicate filamented glass pipettes with 5-8 MΩ resistance and filled with Normal Rat Ringer (in mM: 135 NaCl, 5.4 KCl, 1.8 $CaCl_2$, 1 $MgCl_2$,

5 HEPES) were used to record from individual neuros across the cortical depth of PPC. Pipette solution was supplemented with 20 mg ml^{-1} biocytin to allow extracellular deposits (Moore et al, JoVE) or dye-loading of recorded neurons for post hoc staining to determine its position with respect to the barrel cortex anatomical landmarks (Pinault, JNeurosci 1996, Narayanan et al, JoVE). Cell search was performed while monitoring electrode resistance to record from an unbiased sample of PPC neurons, independent of spiking frequencies of individual neurons.

Spontaneous activity was first recorded for 100 seconds for each neuron, followed by whisker stimulation, where individual whiskers were subsequently deflected using a piezoelectric bimorph attached to a glass capillary. Individual whiskers were deflected 20x in the rostro-caudal direction at 3.3 degrees with an onset-offset interval of 200 ms and an inter trial interval of 2000 ms. All recordings consisted of a single unit with positive going action potentials as well as local field potentials obtained through the juxtasomal electrode. Control trials involved comparable experimental protocols but with the glass capillary just outside the whisker tip to simulate stimulation conditions without somatosensory information. Recordings were made using an Axoclamp 2B amplifier (Axon instruments, Union City, CA, US) along with a Lynx 8 amplifier filtered between 300 Hz and 9000 Hz. We used custom made software on Labview (National Instruments. Austin, TX, USA) to acquire data (nTrode, Randy Bruno, Columbia University, NY, USA). Spikes were sorted offline using Mclust 2.0 (A.David Redish, University of Minnesota, Minneapolis, USA).

Histology and reconstruction

The histology procedure used to reveal anatomical landmarks and recorded neurons has previously been described (Wong-Riley 1979; Horikawa and Armstrong 1988; Narayanan *et al.* 2014). Briefly, animals were transcardially perfused with 0.1M phosphate buffered saline (pH 7.2) followed by 4% paraformaldehyde (PFA) and brains were removed and fixed in PFA for 24 hours. Twenty-four 100 µm tangential sections were obtained and Cytochrome oxidase staining was used on sections 6-11 to reveal anatomical landmarks in primary somatosensory cortex (S1). The chromagen 3,3' diaminobenzidine tetrahydrochloride (DAB) staining was using to reveal dendritic architecture and position of recorded neurons with respect to S1. For a subset of recordings, barrel architecture, slice boundaries and cell location were reconstructed in 3D under a bright field microscope using Neurolucida software (Microbrightfield, Williston, VT, USA).

Data analysis of juxtasomal recordings in anaesthetized animals.

Activity evoked by single whisker stimulation was quantified by analyzing the action

potentials (APs) observed during onset of whisker deflection (200ms) and averaged over 20 trials. Spontaneous activity measurements used to evaluate evoked response was calculated by quantifying APs 0-100 ms prior to whisker deflection and averaged over 20 trials for all whiskers. Evoked response for a single whisker was corrected for spontaneous activity and evoked response for individual whiskers was used to build receptive field maps of individual neurons in PPC. To determine whether the evoked activity was significantly different from spontaneous activity, the spiking per whisker was binned into 10 ms bins. The spontaneous spiking was modeled as a Poisson distribution and then checked for bins during evoked activity that significantly exceeded the pre-stimulus spontaneous distribution ($p<0.01$) (de Kock *et al.* 2007). The threshold to consider a single neurons response to single whisker stimulation was if evoked activity significantly differed from spontaneous activity and if whisker stimulation evoked APs in 25% of the trials. The LFP intensity maps were constructed by quantifying the integral of the stimulus-evoked LFP in the 0-100 ms post-stimulus window. The LFP receptive field map was generated by plotting the intensity of the LFP response. Mean LFP response intensity was calculated for each row of whiskers per recording location and color-coded corresponding to the row generating maximum mean LFP intensity post deflection.

Awake animal preparation

Male wistar rats (P28 - P42, average +stdev) were used for juxtasomal single cell (n=10) and silicon probe multiunit (n=2) recordings during free whisking and novel object touch behavior. During surgery, animals were anaesthetized with 1.5% isoflurane in 0.4 l/h O_2 and 0.7 l/h NO_2. The skull over the PPC in the left hemisphere was thinned at 3.5 mm posterior to Bregma and 4.5 mm lateral from mid line and protected using a plastic cylinder and screw cap. A metal head post was firmly attached to the skull using dental cement (Tetric EvoFlow, Ivoclar Vivadent AG) after which rats were allowed to recover for 24 hours (Boudewijns et al. 2013; Narayanan *et al.* 2014). Animals were habituated to head fixation by daily trainings with increasing duration (5-25 min). Rats were housed in enriched cages (shelter, bedding material, toys) and body weight monitored throughout the entire experimental procedure. Recording sessions were initiated when rats were habituated to head-fixation.

Unit recording in awake cortex

On the recording day, the rat was anaesthetized with 1.5% isoflurane (0.4 l/h O_2 and 0.7 l/h NO_2) and a craniotomy performed over the thinned region of interest. Borosilicate glass pipettes, as described previously, were used to record from individual neurons. While recording, whiskers were individually deflected using a glass capillary attached

to a bimorph piezo to find the whisker row generating strongest LFP activity. Either two whiskers (n=1) belonging to arc 0 and 1 or three whiskers (n=8) with arc 0,1 or 2 of that row were clipped to a length of 30- 35 mm and all other whiskers were clipped close to the whisker follicle. Spontaneous activity was recorded for 100 s followed by biocytin filling session (Pinault 1996; Narayanan *et al.* 2014). Afterwards, neurons were allowed to recover from the filling procedure until pre-filling spiking conditions were re-established. Anesthesia was then stopped and animal was allowed to wake up while continuing the recording. The rat was allowed to whisk and touch a novel cylindrical metal pole positioned within reach of the spared whisker, which the animal could touch with its whiskers voluntarily. Whisking and touch behavior was recorded at 200 Hz using a Nikon AF Nikkor 50mm f/1.4D camera placed over head and illuminated with red led lights. Whisker position was tracked off-line using Matlab based software WhiskerTracker (Knutsen et al. 2005) and python based "whisk" (Clack et al. 2012). Touch start and end times were obtained by manual inspection of video files frame-by-frame.

Multiunit activity was recorded using probes (E32-50-S1-L6, Atlas Neuroengineering, Leuven, Belgium) with 32 Iridium oxide electrodes bearing a pitch of 50 µm, spanning 1550 µm and divided into 8 tetrodes. Probes coated with dil were inserted to a depth of 1900 µm from the pia and multiunit activity recorded first during free whisking and then during object touch behavior as described above. Multiunit activity was acquired at 30 KHz using open ephys acquisition board and recorded using open ephys GUI software (website reference). The online signal was bandpass filtered (0.3 – 6 KHz) prior to online sorting. Whisking and touch behavior was captured at 400 Hz using a camera as described above. Additionally prior to object touch behavior session, rats were also allowed to freely whisk during which there was no object with in its whisking field while recording.

Histology

Brains were removed and sliced for histology, as described earlier (Boudewijns *et al.* 2013; Narayanan *et al.* 2014). Cytochrome oxidase followed by DAB staining for single cell morphology was used to identify PPC recording site with respect to barrel cortex for juxtasomal recordings. For multiunit probe recordings, cytochrome oxidase staining was performed as described earlier. Tangential sections were viewed under fluorescence microscope to reveal DiI staining of silicon probe track and its position with respect to barrel cortex.

Single and multiunit spike sorting

Spike sorting for juxtasomal recording of single cells was performed in Mclust 2.0

through manual clustering. Spike sorting for multiunit recording was performed in Mclust 4.3 (Fraley and Raftery 2002, 2003) with units first clustered semi-automatically using klustakwik (Harris et al. 2000) followed by manual clustering. Spike sorting was performed based on previously described methods (Csicsvari et al. 1999; Harris et al. 2001; Bartho *et al.* 2004; Harris et al. 2016). For clustering, channels were grouped into a tetrode format, where four linearly arranged consecutive channels were used to sort units online. Online sorted units from each tetrode configuration were further semi-automatically sorted first using klustakwik to obtain L-ratios (LR) and Isolation distance (ID) for all clusters. Only units with ID's greater than 8 were further used for manual sorting. About 94 % of units had ID's greater than 10. Isolated units were then manually checked for various parameters including spikes within refractory period of 2 ms, spike shapes, auto correlations, inter spike intervals and presence of the unit during entire recording session (Csicsvari *et al.* 1999; Harris *et al.* 2001; Bartho *et al.* 2004; Reyes-Puerta *et al.* 2015; Harris *et al.* 2016). Only clusters that could be well identified as a putative unit were further used for all analysis.

Cell type identification was performed as described previously (Bartho *et al.* 2004). Briefly, half width and trough to peak latency was measured for each unit. Unsupervised cluster analysis was performed based on Euclidean distance between the two parameters and number of significant clusters defining cell types were determined by Thorndike procedure (Thorndike 1953). Clusters were defined as putative pyramidal and putative interneurons based on previously described nomenclature (Bartho *et al.* 2004). All statistical measures were performed using Matlab (Mathworks, 2014a).

Acknowledgment

We would like to thank Fritjof Helmchen and Jochen Staiger for the informative discussions thah helped conduct the project.

References

Aflalo T, Kellis S, Klaes C, Lee B, Shi Y, Pejsa K, Shanfield K, Hayes-Jackson S, Aisen M, Heck C, Liu C, Andersen RA. 2015. Neurophysiology. Decoding motor imagery from the posterior parietal cortex of a tetraplegic human. Science 348:906-910.

Ahissar E, Sosnik R, Haidarliu S. 2000. Transformation from temporal to rate coding in a somatosensory thalamocortical pathway. Nature 406:302-306.

Alloway KD. 2008. Information processing streams in rodent barrel cortex: the differential functions of barrel and septal circuits. Cereb Cortex 18:979-989.

Andersen RA. 1997. Multimodal integration for the representation of space in the posterior parietal cortex. Philos Trans R Soc Lond B Biol Sci 352:1421-1428.

Andersen RA, Cui H. 2009. Intention, action planning, and decision making in parietal-frontal circuits. Neuron 63:568-583.

Andersen RA, Snyder LH, Bradley DC, Xing J. 1997. Multimodal representation of space in the posterior parietal cortex and its use in planning movements. Annu Rev Neurosci 20:303-330.

Avillac M, Ben Hamed S, Duhamel JR. 2007. Multisensory integration in the ventral intraparietal area of the macaque monkey. J Neurosci 27:1922-1932.

Bartho P, Hirase H, Monconduit L, Zugaro M, Harris KD, Buzsaki G. 2004. Characterization of neocortical principal cells and interneurons by network interactions and extracellular features. J Neurophysiol 92:600-608.

Bensmaia SJ, Miller LE. 2014. Restoring sensorimotor function through intracortical interfaces: progress and looming challenges. Nat Rev Neurosci 15:313-325.

Bosman LW, Houweling AR, Owens CB, Tanke N, Shevchouk OT, Rahmati N, Teunissen WH, Ju C, Gong W, Koekkoek SK, De Zeeuw CI. 2011. Anatomical pathways involved in generating and sensing rhythmic whisker movements. Front Integr Neurosci 5:53.

Boudewijns ZS, Groen MR, Lodder B, McMaster MT, Kalogreades L, de Haan R, Narayanan RT, Meredith RM, Mansvelder HD, de Kock CP. 2013. Layer-specific high-frequency action potential spiking in the prefrontal cortex of awake rats. Front Cell Neurosci 7:99.

Brecht M, Krauss A, Muhammad S, Sinai-Esfahani L, Bellanca S, Margrie TW. 2004. Organization of rat vibrissa motor cortex and adjacent areas according to cytoarchitectonics, microstimulation, and intracellular stimulation of identified cells. J Comp Neurol 479:360-373.

Brecht M, Schneider M, Sakmann B, Margrie TW. 2004. Whisker movements evoked by stimulation of single pyramidal cells in rat motor cortex. Nature 427:704-710.

Chandler HC, King V, Corwin JV, Reep RL. 1992. Thalamocortical connections of rat posterior parietal cortex. Neurosci Lett 143:237-242.

Chen JL, Carta S, Soldado-Magraner J, Schneider BL, Helmchen F. 2013. Behaviour-dependent recruitment of long-range projection neurons in somatosensory cortex. Nature 499:336-340.

Chen JL, Voigt FF, Javadzadeh M, Krueppel R, Helmchen F. 2016. Long-range population dynamics of anatomically defined neocortical networks. Elife 5.

Chen LL, Lin LH, Barnes CA, McNaughton BL. 1994. Head-direction cells in the rat posterior cortex. II. Contributions of visual and ideothetic information to the directional firing. Exp Brain Res 101:24-34.

Chen LL, Lin LH, Green EJ, Barnes CA, McNaughton BL. 1994. Head-direction cells in the rat posterior cortex. I. Anatomical distribution and behavioral modulation. Exp Brain Res 101:8-23.

Clack NG, O'Connor DH, Huber D, Petreanu L, Hires A, Peron S, Svoboda K, Myers EW. 2012. Automated tracking of whiskers in videos of head fixed rodents. PLoS Comput Biol 8:e1002591.

Colechio EM, Alloway KD. 2009. Differential topography of the bilateral cortical projections to the whisker and forepaw regions in rat motor cortex. Brain Struct Funct 213:423-439.

Csicsvari J, Hirase H, Czurko A, Mamiya A, Buzsaki G. 1999. Oscillatory coupling of hippocampal pyramidal cells and interneurons in the behaving Rat. J Neurosci 19:274-287.

Cui H, Andersen RA. 2007. Posterior parietal cortex encodes autonomously selected motor plans. Neuron 56:552-559.

Cullen KE. 2004. Sensory signals during active versus passive movement. Curr Opin Neurobiol 14:698-706.

Curtis JC, Kleinfeld D. 2009. Phase-to-rate transformations encode touch in cortical neurons of a scanning sensorimotor system. Nat Neurosci 12:492-501.

de Kock CP, Bruno RM, Spors H, Sakmann B. 2007. Layer- and cell-type-specific suprathreshold stimulus representation in rat primary somatosensory cortex. J Physiol 581:139-154.

de Kock CP, Sakmann B. 2009. Spiking in primary somatosensory cortex during natural whisking in awake head-restrained rats is cell-type specific. Proceedings of the National Academy of Sciences of the United States of America 106:16446-16450.

Diamond ME, Arabzadeh E. 2013. Whisker sensory system - from receptor to decision. Prog Neurobiol 103:28-40.

Diamond ME, von Heimendahl M, Knutsen PM, Kleinfeld D, Ahissar E. 2008. 'Where' and 'what' in the whisker sensorimotor system. Nat Rev Neurosci 9:601-612.

Egger R, Narayanan RT, Helmstaedter M, de Kock CP, Oberlaender M. 2012. 3D reconstruction and standardization of the rat vibrissal cortex for precise registration of single neuron morphology. PLoS Comput Biol 8:e1002837.

Feldmeyer D, Brecht M, Helmchen F, Petersen CC, Poulet JF, Staiger JF, Luhmann HJ, Schwarz C. 2013. Barrel cortex function. Prog Neurobiol 103:3-27.

Fox MT, Barense MD, Baxter MG. 2003. Perceptual attentional set-shifting is impaired in rats with neurotoxic lesions of posterior parietal cortex. J Neurosci 23:676-681.

Fraley C, Raftery AE. 2002. Model-based clustering, discriminant analysis, and density estimation. J Am Stat Assoc

97:611-631.

Fraley C, Raftery AE. 2003. Enhanced model-based clustering, density estimation, and discriminant analysis software: MCLUST. J Classif 20:263-286.

Friedman WA, Zeigler HP, Keller A. 2012. Vibrissae motor cortex unit activity during whisking. J Neurophysiol 107:551-563.

Fries P. 2009. Neuronal gamma-band synchronization as a fundamental process in cortical computation. Annu Rev Neurosci 32:209-224.

Gail A, Andersen RA. 2006. Neural dynamics in monkey parietal reach region reflect context-specific sensorimotor transformations. J Neurosci 26:9376-9384.

Hanks TD, Kopec CD, Brunton BW, Duan CA, Erlich JC, Brody CD. 2015. Distinct relationships of parietal and prefrontal cortices to evidence accumulation. Nature 520:220-223.

Harris KD, Henze DA, Csicsvari J, Hirase H, Buzsaki G. 2000. Accuracy of tetrode spike separation as determined by simultaneous intracellular and extracellular measurements. J Neurophysiol 84:401-414.

Harris KD, Hirase H, Leinekugel X, Henze DA, Buzsaki G. 2001. Temporal interaction between single spikes and complex spike bursts in hippocampal pyramidal cells. Neuron 32:141-149.

Harris KD, Quiroga RQ, Freeman J, Smith SL. 2016. Improving data quality in neuronal population recordings. Nat Neurosci 19:1165-1174.

Harvey CD, Coen P, Tank DW. 2012. Choice-specific sequences in parietal cortex during a virtual-navigation decision task. Nature 484:62-68.

Hill DN, Curtis JC, Moore JD, Kleinfeld D. 2011. Primary motor cortex reports efferent control of vibrissa motion on multiple timescales. Neuron 72:344-356.

Hooks BM. 2016. Sensorimotor Convergence in Circuitry of the Motor Cortex. Neuroscientist.

Horikawa K, Armstrong WE. 1988. A versatile means of intracellular labeling: injection of biocytin and its detection with avidin conjugates. J Neurosci Methods 25:1-11.

Knutsen PM, Derdikman D, Ahissar E. 2005. Tracking whisker and head movements in unrestrained behaving rodents. J Neurophysiol 93:2294-2301.

Knutsen PM, Mateo C, Kleinfeld D. 2016. Precision mapping of the vibrissa representation within murine primary somatosensory cortex. Philos Trans R Soc Lond B Biol Sci 371.

Kolb B, Walkey J. 1987. Behavioural and anatomical studies of the posterior parietal cortex in the rat. Behav Brain Res 23:127-145.

Lee T, Alloway KD, Kim U. 2011. Interconnected cortical networks between primary somatosensory cortex septal columns and posterior parietal cortex in rat. J Comp Neurol 519:405-419.

Li N, Daie K, Svoboda K, Druckmann S. 2016. Robust neuronal dynamics in premotor cortex during motor planning. Nature 532:459-464.

Matyas F, Sreenivasan V, Marbach F, Wacongne C, Barsy B, Mateo C, Aronoff R, Petersen CC. 2010. Motor control by sensory cortex. Science 330:1240-1243.

Moore JD, Deschenes M, Kleinfeld D. 2015. Juxtacellular Monitoring and Localization of Single Neurons within Subcortical Brain Structures of Alert, Head-restrained Rats. J Vis Exp.

Moore JD, Mercer Lindsay N, Deschenes M, Kleinfeld D. 2015. Vibrissa Self-Motion and Touch Are Reliably Encoded along the Same Somatosensory Pathway from Brainstem through Thalamus. PLoS Biol 13:e1002253.

Mountcastle VB. 1997. The columnar organization of the neocortex. Brain 120 (Pt 4):701-722.

Mountcastle VB, Lynch JC, Georgopoulos A, Sakata H, Acuna C. 1975. Posterior parietal association cortex of the monkey: command functions for operations within extrapersonal space. J Neurophysiol 38:871-908.

Narayanan RT, Mohan H, Broersen R, de Haan R, Pieneman AW, de Kock CP. 2014. Juxtasomal biocytin labeling to study the structure-function relationship of individual cortical neurons. J Vis Exp:e51359.

Nitz DA. 2006. Tracking route progression in the posterior parietal cortex. Neuron 49:747-756.

Nitz DA. 2012. Spaces within spaces: rat parietal cortex neurons register position across three reference frames. Nat Neurosci 15:1365-1367.

O'Connor DH, Peron SP, Huber D, Svoboda K. 2010. Neural activity in barrel cortex underlying vibrissa-based object localization in mice. Neuron 67:1048-1061.

Oberlaender M, Boudewijns ZS, Kleele T, Mansvelder HD, Sakmann B, de Kock CP. 2011. Three-dimensional axon morphologies of individual layer 5 neurons indicate cell type-specific intracortical pathways for whisker motion and

touch. Proceedings of the National Academy of Sciences of the United States of America 108:4188-4193.

Olcese U, Iurilli G, Medini P. 2013. Cellular and synaptic architecture of multisensory integration in the mouse neocortex. Neuron 79:579-593.

Olsen GM, Witter MP. 2016. The posterior parietal cortex of the rat: architectural delineation and thalamic differentiation. J Comp Neurol.

Petersen CC. 2007. The functional organization of the barrel cortex. Neuron 56:339-355.

Petersen CC. 2014. Cortical control of whisker movement. Annu Rev Neurosci 37:183-203.

Pinault D. 1996. A novel single-cell staining procedure performed in vivo under electrophysiological control: morpho-functional features of juxtacellularly labeled thalamic cells and other central neurons with biocytin or Neurobiotin. J Neurosci Methods 65:113-136.

Reep RL, Chandler HC, King V, Corwin JV. 1994. Rat posterior parietal cortex: topography of corticocortical and thalamic connections. Exp Brain Res 100:67-84.

Reep RL, Corwin JV. 2009. Posterior parietal cortex as part of a neural network for directed attention in rats. Neurobiol Learn Mem 91:104-113.

Reyes-Puerta V, Sun JJ, Kim S, Kilb W, Luhmann HJ. 2015. Laminar and Columnar Structure of Sensory-Evoked Multineuronal Spike Sequences in Adult Rat Barrel Cortex In Vivo. Cereb Cortex 25:2001-2021.

Sakata S, Harris KD. 2009. Laminar structure of spontaneous and sensory-evoked population activity in auditory cortex. Neuron 64:404-418.

Smith JB, Alloway KD. 2013. Rat whisker motor cortex is subdivided into sensory-input and motor-output areas. Front Neural Circuits 7:4.

Snyder LH, Batista AP, Andersen RA. 1997. Coding of intention in the posterior parietal cortex. Nature 386:167-170.

Snyder LH, Batista AP, Andersen RA. 1998. Change in motor plan, without a change in the spatial locus of attention, modulates activity in posterior parietal cortex. J Neurophysiol 79:2814-2819.

Thorndike RL. 1953. Who belongs in the family? Psychometrika 18:10.

Torrealba F, Valdes JL. 2008. The parietal association cortex of the rat. Biol Res 41:369-377.

Urbain N, Salin PA, Libourel PA, Comte JC, Gentet LJ, Petersen CC. 2015. Whisking-Related Changes in Neuronal Firing and Membrane Potential Dynamics in the Somatosensory Thalamus of Awake Mice. Cell Rep 13:647-656.

Velez-Fort M, Rousseau CV, Niedworok CJ, Wickersham IR, Rancz EA, Brown AP, Strom M, Margrie TW. 2014. The stimulus selectivity and connectivity of layer six principal cells reveals cortical microcircuits underlying visual processing. Neuron 83:1431-1443.

Wang Q, Sporns O, Burkhalter A. 2012. Network analysis of corticocortical connections reveals ventral and dorsal processing streams in mouse visual cortex. J Neurosci 32:4386-4399.

Whitlock JR. 2014. Navigating actions through the rodent parietal cortex. Front Hum Neurosci 8:293.

Whitlock JR, Sutherland RJ, Witter MP, Moser MB, Moser EI. 2008. Navigating from hippocampus to parietal cortex. Proceedings of the National Academy of Sciences of the United States of America 105:14755-14762.

Wimmer VC, Bruno RM, de Kock CP, Kuner T, Sakmann B. 2010. Dimensions of a projection column and architecture of VPM and POm axons in rat vibrissal cortex. Cereb Cortex 20:2265-2276.

Wong-Riley M. 1979. Changes in the visual system of monocularly sutured or enucleated cats demonstrable with cytochrome oxidase histochemistry. Brain Res 171:11-28.

Woolsey TA, Van der Loos H. 1970. The structural organization of layer IV in the somatosensory region (SI) of mouse cerebral cortex. The description of a cortical field composed of discrete cytoarchitectonic units. Brain Res 17:205-242.

Yamashita T, Petersen C. 2016. Target-specific membrane potential dynamics of neocortical projection neurons during goal-directed behavior. Elife 5.

Yang H, Kwon SE, Severson KS, O'Connor DH. 2016. Origins of choice-related activity in mouse somatosensory cortex. Nat Neurosci 19:127-134.

Yu C, Derdikman D, Haidarliu S, Ahissar E. 2006. Parallel thalamic pathways for whisking and touch signals in the rat. PLoS Biol 4:e124.